Macromolecules

pubs.acs.org/Macromolecules

Article

# Impact of the Environment on the PNIPAM Dynamical Transition Probed by Elastic Neutron Scattering

Benedetta P. Rosi, Arianna D'Angelo, Elena Buratti, Marco Zanatta, Letizia Tavagnacco, Francesca Natali, Michaela Zamponi, Daria Noferini, Silvia Corezzi, Emanuela Zaccarelli, Lucia Comez, Francesco Sacchetti, Alessandro Paciaroni, Caterina Petrillo, and Andrea Orecchini*

Cite This: *Macromolecules* 2022, 55, 4752–4765

Read Online

ACCESS | Metrics & More | Article Recommendations | Supporting Information

**ABSTRACT:** By means of elastic incoherent neutron scattering, we investigated how the addition of stabilizing cosolvents (glycerol and glucose) affects the dynamics of hydrated PNIPAM chains at the pico- and nanosecond time scale, where a low-temperature dynamical transition is observed. From the elastic intensities, the atomic mean square displacements of the PNIPAM samples were extracted using a global fitting procedure. Both the dynamical transition temperature $T_d$ and the amplitude of the displacements are found to be strongly dependent on solvent composition. The close analogies between the dynamical transition of PNIPAM and that of biomolecules reveal PNIPAM as an excellent system for reproducing complex solvent−biopolymer interactions.

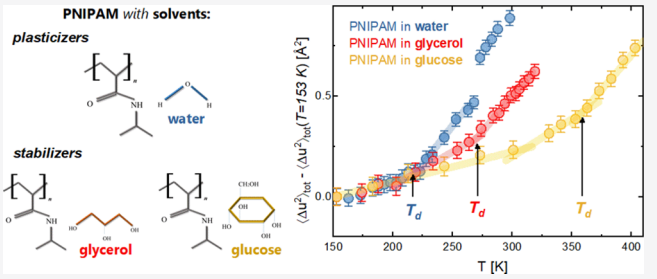


## 1. INTRODUCTION

Smart responsive polymers are a subject of strong interest within the scientific community due to their ability to undergo drastic changes in response to variations of external parameters, such as temperature, pH, or solvent composition.[1] A paradigmatic example of smart polymers is poly-*N*-isopropylacrylamide (PNIPAM), whose repeating unit includes both hydrophilic amide and hydrophobic isopropyl groups (Scheme 1). The resulting amphiphilic nature produces inverse solubility in water upon heating and triggers a coil-to-globule transition of the polymer at a lower critical solution temperature (LCST) of about 305 K.[2] The LCST located between room and body temperature makes PNIPAM versatile for biological and biomedical applications, ranging from tissue engineering to drug delivery.[3−6]

In a similar context of biophysical interest, PNIPAM has raised further attention as a simple but predictive protein model, since the coil-to-globule transition in many aspects resembles the cold renaturation of small globular proteins.[7−14] From a fundamental point of view, the availability of such a model system would provide unique opportunities to reproduce, better understand, and fine tune the essential elements at the basis of complex biological mechanisms. From a technological point of view, the perspective of functionalizing PNIPAM to replicate specific biological processes may have a huge impact, for instance, on large-scale applications and analysis. Indeed, the extensive use of natural enzymes is often limited by high costs, demanding storage conditions, and poor availability due to the usually low yield of protein expression. These shortcomings could be overcome by exploiting the

**Scheme 1. Chemical Formula of the NIPAM Repeating Unit**[a]

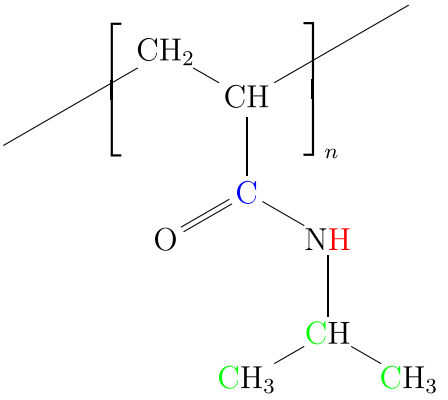


[a]The C atoms of the amide (hydrophilic) and isopropyl (hydrophobic) groups in the side chain are highlighted in blue and green, respectively. The exchangeable H atom in the amide group is highlighted in red.

Received: January 24, 2022
Revised: May 4, 2022
Published: June 1, 2022

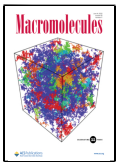







https://doi.org/10.1021/acs.macromol.2c00177
*Macromolecules* 2022, 55, 4752−4765

Table 1. List of Samples Together with Specific Details of Sample Preparation and Other Experimental Information

| | | | | | | $\mathcal{T}$ [K][f] | |
|---|---|---|---|---|---|---|---|
| sample | $h$[a] $\left[\frac{\text{mg of water}}{\text{mg of PNIPAM}}\right]$ | $\frac{m_c}{m_p}\left[\frac{\text{mg of cosolvent}}{\text{mg of PNIPAM}}\right]$[b] | $t$[c] [mm] | $\mathcal{T}$ [%][d] | $\left[\frac{\sigma_{inc}}{\sigma_{tot}}\right]$ [%][e] | IN13 $\tau_R$ = 150 ps | SPHERES $\tau_R$ = 2000 ps |
| PNIPAM 0$h$ | 0.05 | | 0.2 | 90.7 | 92 | 153−313 | 20, 153−298 |
| PNIPAM 1$h$ | 1.00 | | 0.3 | 91.6 | 84 | 153−298 | 20, 153−298 |
| PNIPAM:d-glyc 0$h$ | 0.05 | 1 | 0.3 | 92.7 | 84 | 153−318 | 20, 153−318 |
| PNIPAM:d-glyc 0.15$h$ | 0.15 | 1 | 0.3 | 92.2 | 83 | 153−318 | 20, 153−298 |
| PNIPAM:d-glyc 0.35$h$ | 0.35 | 1 | 0.4 | 90.7 | 82 | 153−318 | 20, 153−298 |
| PNIPAM:d-glyc 1$h$ | 1.00 | 1 | 0.4 | 92.1 | 78 | 153−318 | 20, 153−298 |
| PNIPAM:d-glu 0$h$ | 0.05 | 1 | 0.3 | 90.6 | 85 | 153−403 | 20, 153−418 |
| PNIPAM:d-glu 0.15$h$ | 0.15 | 1 | 0.3 | 90.5 | 84 | 153−393 | 20, 153−398 |
| PNIPAM:d-glu 0.35$h$ | 0.35 | 1 | 0.3 | 92.0 | 82 | 153−318 | 20, 153−298 |
| PNIPAM:d-glu 1$h$ | 1.00 | 1 | 0.4 | 90.6 | 78 | 153−318 | 20, 153−298 |

[a]Measured value of hydration degree. The estimated relative error is of about 5%. [b]Cosolvent/PNIPAM weight ratio. [c]Cell inner thickness. [d]Theoretical neutron transmission. [e]Ratio between incoherent and total scattering cross section. [f]Measured temperature ranges.

higher chemical stability and malleability, abundance, and cheapness of PNIPAM-based systems.[15−17]

Although interest in the coil-to-globule transition has produced vast literature on the behavior of PNIPAM solutions in diluted regime and around room temperature,[18] other regions of the phase diagram are largely unexplored. Only recently, neutron scattering experiments and molecular dynamics simulations disclosed the existence of a dynamical transition in weakly hydrated PNIPAM samples at a critical temperature $T_d \approx 220$ K.[19−21] Originally observed in proteins[22,23] and later in DNA[24,25] and t-RNA,[26,27] the dynamical transition is a well-known phenomenon in the physics of hydrated biomolecules, whose origin is still widely debated.[28−30] It appears as a slope change at $T_d$ in the temperature dependence of the atomic mean square displacements (MSDs) of the macromolecule. Above $T_d$, activation of conformational degrees of freedom takes place, resulting in a faster increase with temperature of the MSDs on the picosecond and nanosecond time scales and a correspondingly enhanced molecular flexibility. Common features of the transition, manifested by both biopolymers and PNIPAM, are (i) the intimate coupling between solvent and solute dynamics, attested by the occurrence of an analogous dynamical transition in the hydration water of the macromolecule[20,31] and by the progressive disappearance of the transition upon dehydration, and (ii) the connection with the inherent complexity of the polymer repeating unit rather than with the mesoscopic architecture of the whole macromolecule. Indeed, the PNIPAM dynamical transition occurs in both linear chains[19] and microgel networks.[21] Likewise, the transition is observed not only in proteins and nucleic acids but also in amyloid fibrils and even in unbound amino acids.[32,33]

For biological molecules, the possibility of regulating the conformational flexibility across the dynamical transition is of great importance. On one hand, the degree of flexibility achieved thanks to fast picosecond to nanosecond motions is essential for biological agents to reach functionality and the necessary reaction rates at physiological temperatures.[34−38] On the other hand, controlled flexibility and limited biological activity are desirable in the context of protein storage, transport, and delivery because they allow better preservation from denaturation in the case of hostile external conditions, such as high temperatures or low pH. In medicine and pharmaceutics, for instance, careful regulation of the enzyme activity is crucial to improve the shelf life of protein-based drugs.[39−41]

Many ongoing studies aim at elucidating how the atomic motions and conformational flexibility of proteins can be controlled by properly tuning the characteristics of their solvent environment. Water, the main physiological milieu of biomolecules, is well known as the archetype of plasticizers, i.e., the class of solvents that impart the flexibility needed to undergo the dynamical transition and eventually perform biological functions. On the contrary, protein solvation by stabilizing additives, such as sugars and polyols, results in a stiffening of the molecular motions and leads to either a shift of $T_d$ toward higher temperatures or complete suppression of the transition.[42−49] Stabilizers are routinely exploited for long-term protein storage,[50] thus reinforcing the connection between molecular flexibility at the picosecond to nanosecond time scale and stability at the macroscopic level.[51,52] Detailed knowledge of how different classes of solvents affect the fast dynamics of macromolecules is therefore of paramount importance. Although the relevant existing literature is wide and keeps growing, the details of the underlying mechanisms are still much debated.

From the perspective of exploiting PNIPAM-based systems as protein analogues, the study of the dynamical transition of PNIPAM in the presence of plasticizing or stabilizing solvents acquires a relevant and 2-fold value. On one hand, it can provide new insights onto the solute−solvent interactions at the basis of the dynamical transition observed in complex macromolecules. On the other hand, this study will help to push further the PNIPAM−protein analogy and possibly open new routes to artificially replicate biological functions by means of tailored smart materials.

In this work, we study how the addition of stabilizing agents, like sugars (glucose) and polyols (glycerol), impacts the dynamical transition of hydrated PNIPAM chains. For this purpose, we performed an extensive campaign of elastic incoherent neutron scattering (EINS) measurements that allowed us to derive the MSDs of PNIPAM in a time interval ranging from 150 to 2000 ps. From the analysis of both EINS intensities and MSDs, a coherent picture emerged about the impact that the solvent characteristics have on both the onset temperature of the dynamical transition and the amplitude of the relevant atomic motions. We found that when the polymer is embedded in glycerol or glucose, the dynamical transition occurs even in the absence of water, although an upshift of the


https://doi.org/10.1021/acs.macromol.2c00177
Macromolecules 2022, 55, 4752−4765

transition temperature $T_d$ is observed. In the presence of binary solvent mixtures, the competition between water and cosolvent in interaction with PNIPAM results in a strong dependence of $T_d$ on the water content. Water−PNIPAM interactions appear favored down to rather low hydration levels, suggesting a preferential affinity of the polymer for water molecules. Remarkably, the comparison with proteins reveals the existence of strong analogies between PNIPAM and protein behavior, not only in purely hydrated conditions but even in the presence of more complex solvent environments.

## 2. MATERIALS AND METHODS

**2.1. Samples.** PNIPAM linear chains (number-averaged molecular weight $M_n$ = 40 kDa), glucose-1,2,3,4,5,6,6-$d_7$ (97 atom % D), and glycerol-$d_8$ (≥98 atom % D) were purchased from Sigma-Aldrich. Deuterium oxide ($D_2O$, 99.96 atom % D) was purchased from Cambridge Isotopes Laboratories, Inc. Samples of PNIPAM, PNIPAM in deuterated glycerol (PNIPAM:d-glyc), and PNIPAM in deuterated glucose (PNIPAM:d-glu) were prepared at different values of hydration degree $h$, defined as the ratio $\frac{m_w}{m_p}$ between the mass of heavy water $m_w$ and the mass of PNIPAM $m_p$. From here onward, the hydration degree $h$ = 0.35, for instance, will be referred to as 0.35$h$. The list of prepared samples together with the corresponding hydration degree and other relevant experimental details is reported in Table 1. Each sample was prepared starting with the same amount of PNIPAM $m_p \approx 250$ mg. An equal amount of cosolvent $m_c \approx 250$ mg was added where required in order to have a fixed 1:1 weight ratio with PNIPAM, in analogy with the procedure typically used for the preparation of protein−glycerol and protein−glucose mixtures.[44,53] The powder samples were then dissolved in ≈5 g of $D_2O$ and cool stored at about 277 K for 2 days to ensure that all exchangeable hydrogen atoms were properly substituted with deuterium. The samples were subsequently freeze dried and then further dehydrated under vacuum in the presence of $P_2O_5$ until a stable dry weight was achieved. The dry samples were put in the presence of $D_2O$ vapor until the desired value of $h$ was reached. Samples were finally sealed with indium wire in standard aluminum flat cells. For PNIPAM:d-glu 0$h$ and 0.15$h$, a lead wire was used instead to allow these two samples to be measured up to higher temperatures (see Table 1). The inner thickness $t$ of each cell was individually chosen to obtain a theoretical neutron transmission $\mathcal{T}$ of about 90% for every sample (see Table 1).

**2.2. Elastic Incoherent Neutron Scattering Concepts.** In neutron scattering experiments, the observable quantity is the dynamic structure factor $S(\mathbf{Q}, E)$, which provides the probability for a neutron impinging on the sample to be scattered with a wavevector transfer $\mathbf{Q}$ and an exchanged energy $E$. For isotropic (amorphous) samples, like those considered in this study, the dynamic structure factor only depends on the magnitude $Q$ of the wavevector transfer. The interaction of (thermal) neutrons with matter is such that $S(\mathbf{Q}, E)$ contains both coherent scattering contributions, arising from spatial correlations between different atoms as a function of time, and incoherent scattering contributions, due to spatial correlations of a single atom with itself as a function of time and averaged over all atoms. As such, the two contributions provide information about collective and individual atomic movements, respectively.

Since the incoherent scattering cross section of hydrogen ($\sigma_{inc}^{H} \approx$ 80 barn) is much larger than both the coherent and the incoherent cross sections of any other element (a few barns), the incoherent contribution of the hydrogen atoms is largely dominant in our samples (see Table 1). In particular, we exploited the large difference between the hydrogen and the deuterium cross section ($\sigma_{tot}^{D} \approx 8$ barn) by using deuterated solvents and cosolvents, to highlight the dynamics of PNIPAM nonexchangeable H atoms with respect to the dynamics of the solvent constituents. As H atoms are uniformly distributed over the polymer repeating unit (see Scheme 1), eventually they bear information about the dynamics of the PNIPAM chains as a whole.

In a real experiment, the measured dynamic structure factor is convoluted with the resolution function of the employed spectrometer. In the energy domain, the resolution function in the proximity of the elastic peak can often be approximated by a Gaussian shape, characterized by a full width at half-maximum (fwhm) $\Delta E$, whose value depends on the chosen spectrometer and setup and which also defines the instrumental resolution time scale $\tau_R \approx \frac{2\hbar}{\Delta E}$. In the case of elastic incoherent neutron scattering (EINS), the convolution with the resolution function implies that the dynamic structure factor is measured and integrated within a narrow energy window $|E| \lesssim \Delta E$ around the elastic condition $E$ = 0. The resulting EINS intensity $S_{\tau_R}(Q)$ is named "elastic" in the sense that only sample atomic motions with characteristic time scales slower than $\tau_R$—and thus closer in energy to the elastic line—contribute to the measured signal, whereas faster motions fall outside the measured energy window. Any physical or chemical process inducing an increase of atomic mobility, such that the time scales of the involved motions change from larger to smaller values than $\tau_R$, results in a decrease of $S_{\tau_R}(Q)$.

**2.3. Elastic Incoherent Neutron Scattering Experiments.** EINS intensities were collected on two neutron backscattering spectrometers with different energy resolutions $\Delta E$, namely, SPHERES,[54,55] operated by JCNS at the Heinz Maier−Leibnitz Zentrum (MLZ) in Garching (Germany), and IN13,[56] at the Institut Laue−Langevin (ILL) in Grenoble (France). SPHERES is characterized by an incident energy $E_i$ = 2.08 meV and a resolution time scale $\tau_R$ of about 2000 ps ($\Delta E \approx 0.6$ $\mu$eV fwhm). Data were collected in the available range of exchanged momentum $Q$ between 0.22 and 1.84 Å$^{-1}$. Compared to SPHERES, IN13 is characterized by a higher incident energy $E_i$ = 16.45 meV, which allows one to explore a wider $Q$ range between 0.19 and 4.99 Å$^{-1}$. The resolution time scale of IN13 is $\tau_R \approx 150$ ps ($\Delta E \approx 8$ $\mu$eV fwhm).

The temperature ranges in which the samples were measured are reported in Table 1. On IN13, EINS intensities were collected in constant temperature acquisitions with $\Delta T$ steps ranging between 5 and 30 K depending on the expected temperature evolution of each sample. On SPHERES, thanks to its higher flux, EINS intensities were collected along temperature ramps with a 0.23 K/min heating rate, resulting in acquisition steps of about 2 K. EINS intensities on SPHERES were also collected at $T$ = 20 K in order to have a low-temperature value for data normalization.

Transmission measurements confirmed the values calculated for the chosen sample thicknesses (as reported in Table 1). Data were corrected for cell scattering, self-shielding, and detector efficiency by vanadium (IN13) or low-temperature (SPHERES) normalization, whereas multiple-scattering events were neglected. Noisy detectors, mostly located at the highest and lowest angles, were removed. The fully corrected data finally span the $Q$ ranges 1.27−3.93 Å$^{-1}$ for IN13 and 0.60−1.76 Å$^{-1}$ for SPHERES.

**2.4. Fitting Model.** From the EINS intensities, the atomic MSDs can be derived by assuming specific functional forms for $S_{\tau_R}(Q)$ depending on the type of active motions. At sufficiently low temperatures, large-amplitude macromolecular motions are essentially frozen and only small-amplitude harmonic vibrations can take place, which are properly described by a set of quantized harmonic oscillators.[57] In this case, $S_{\tau_R}(Q)$ takes a Gaussian $Q$ dependence[58]

$$S_{\tau_R}(Q) = S_0 e^{-\frac{Q^2}{6}A(T)} \quad (1)$$

where $S_0$ is an intensity prefactor accounting for instrumental details. The term $A(T)$ is proportional to the harmonic MSD, which can be assumed to increase roughly linearly with temperature,[59] according to the well-known Debye model.[60] The Gaussian approximation is strictly valid only at low $Q$ values.[61] Moreover, it becomes more and more inadequate on increasing temperature because a variety of nonharmonic motions, such as diffusions, relaxations, side-chain fluctuations, and structural and conformational transitions, become progressively active. The larger number of degrees of freedom allows


https://doi.org/10.1021/acs.macromol.2c00177
Macromolecules 2022, 55, 4752−4765

the macromolecule to assume many equivalent local configurations (or conformational substates[62]) while maintaining the same coarse structure. The wider exploration of conformational space can be described in a simplified way as jumps between two potential wells separated by an effective distance $d$. Such a double-well model has been successfully used to describe the dynamical transition of biomolecules including proteins,[43,44,53,63] homomeric polypeptides,[64] and DNA[24] as well as that of PNIPAM microgels[21] and linear chains.[19] In this model, $S_{\tau_R}(Q)$ takes the form[65]

$$S_{\tau_R}(Q) = S_0 e^{-\frac{Q^2}{6}A(T)}\left[1 - 2p_1p_2\left(1 - \frac{\sin(Qd)}{Qd}\right)\right] \quad (2)$$

where $p_1$ and $p_2$ are the probabilities of finding the atom in the ground and excited wells, respectively.

Using a Gaussian approximation, the 3-dimensional, isotropic MSDs $\langle \Delta u^2 \rangle_{tot}$ can be written as[19,45]

$$\langle \Delta u^2 \rangle_{tot} = -6\left(\frac{d \ln S_{\tau_R}(Q)}{d(Q^2)}\right)_{Q=0} = A(T) + 2p_1p_2d^2 \quad (3)$$

Well below the dynamical transition, $\langle \Delta u^2 \rangle_{tot}$ increases approximately linearly with $T$ since the MSDs are dominated by the harmonic term $A(T)$. When the system is heated up, the probability $p_2$ of exploring the excited state increases until the second term in eq 3 becomes dominant, resulting in a steep increase in the slope of $\langle \Delta u^2 \rangle_{tot}$ at $T_d$.

All of the parameters in eq 2 may in principle depend on the temperature, sample composition, or instrumental time scale. Preliminary fitting of the data showed a substantial independence of the distance parameter $d$ from the temperature and solvent composition over the whole set of samples, whereas it significantly depended on the instrumental time scale. At $\tau_R$ = 150 ps, a nearly constant value of $d \approx 1.3$ Å was found for all samples, close to the values of $d$ reported for lysozyme and DNA at the same time scale.[24,44,47,63] At $\tau_R$ = 2000 ps, a larger value of $d \approx 2.4$ Å was found. This is consistent with the basic idea that PNIPAM atoms can span a wider portion of the conformational space over longer time scales. It should be also considered that the intensities collected at $\tau_R$ = 150 and 2000 ps cover a higher and lower $Q$ region, respectively. Correspondingly, the two data sets mainly provide information on shorter and larger length scales, consistent with the obtained values of $d$ (≈1.3 Å at $\tau_R$ = 150 ps, ≈2.4 Å at $\tau_R$ = 2000 ps).

On the basis of these preliminary evaluations, we developed an analysis method to simultaneously fit the whole collection of data, thus significantly improving the final error bars of the resulting MSDs. In setting up such a global fitting procedure, we introduced the following constraints.

(i) The parameter $d$ was assumed to be independent of temperature and solvent composition. The dependence of $d$ on the resolution time scale $\tau_R$ was instead expressed through a diffusion-like form $d = \phi\tau_R^{\xi}$.[64,66] In this formula, $\phi$ is related to a diffusion coefficient and $\xi$ takes into account a possible subdiffusive character.

(ii) The harmonic contribution in eq 3 was assumed to increase linearly with $T$ in the temperature window of interest; therefore, it was expressed as $A(T) = aT + C$. Moreover, we assumed the harmonic dynamics to be equally resolved by the two instruments, since we expect its characteristic time scale to be much faster than the employed $\tau_R$, and thus, the parameters $a$ and $C$ were imposed to be independent of $\tau_R$.

(iii) Considering the above assumptions, $\xi$, $\phi$, $a$, and $C$ were constrained to be global fitting parameters, taking the same value for the whole data set. The probability product $p_1p_2$ and the prefactor $S_0$ were instead unconstrained and left free to vary as a function of $T$, $\tau_R$, and solvent composition.

After several tests, all of the collected intensities were simultaneously fitted over a fixed $Q$ range, namely, between 1.27 and 3.93 Å$^{-1}$ at $\tau_R$ = 150 ps and between 0.60 and 1.42 Å$^{-1}$ at $\tau_R$ = 2000 ps. Examples of the resulting fitting functions are reported in Figure 1 for PNIPAM:d-glyc 1$h$, together with the corresponding experimental EINS intensities. For the sake of comparison, also the purely Gaussian fit is reported. The comparison shows how the double-well model of eq 2 captures much better the behavior of the EINS intensities over the wide explored range of $Q$, $T$, and $h$, especially at high temperatures.

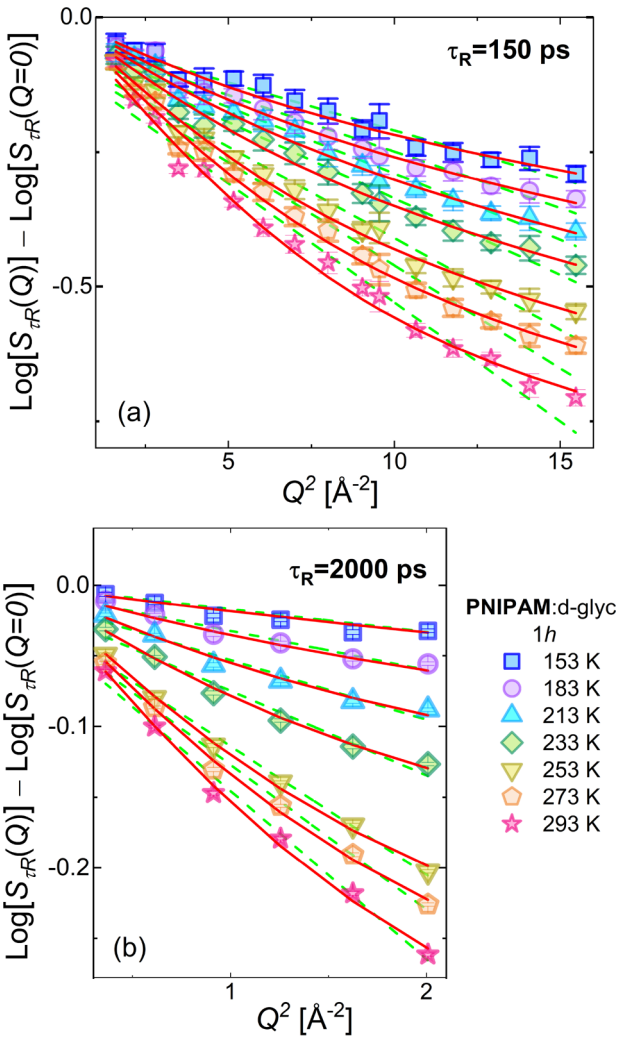


**Figure 1.** Logarithm of the EINS intensities $S_{\tau_R}(Q)$ of PNIPAM:d-glyc 1$h$ as a function of $Q^2$ at selected temperatures. Experimental data are reported together with the double-well fitting functions (solid red lines). For comparison, corresponding Gaussian fitting functions (dashed green lines) are also reported.

The resulting fitting parameters were used to determine the final MSDs by means of eq 3. The MDSs reproduced the behavior qualitatively obtained from the preliminary fit but with clearer and more robust trends. Further details on the data fitting procedure are reported in the Supporting Information.

## 3. RESULTS

### 3.1. Elastic Incoherent Neutron Scattering Intensities.

Preliminary information on the dynamics of PNIPAM is already provided by the inspection of the $Q$-integrated EINS intensities as a function of temperature, $I_{\tau_R}(T)$, reported in Figure 2 for the whole set of samples. For a better comparison between data collected at different $\tau_R$ values, the intensities were obtained by integrating the corresponding $S_{\tau_R}(Q)$ over


https://doi.org/10.1021/acs.macromol.2c00177
Macromolecules 2022, 55, 4752−4765

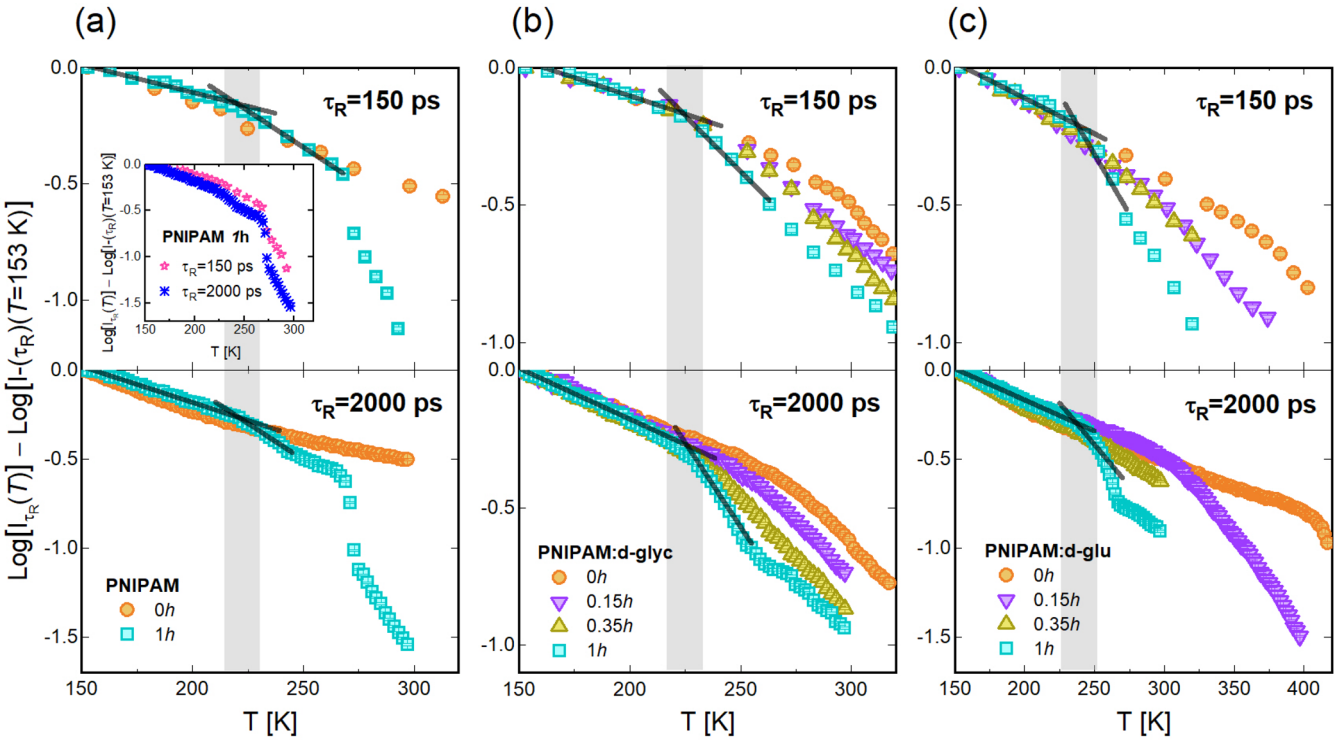


**Figure 2.** Logarithm of the integrated EINS intensities $I_{\tau_R}(T)$ versus $T$ for (a) PNIPAM, (b) PNIPAM:d-glyc, and (c) PNIPAM:d-glu. Data are rescaled by their value at $T$ = 153 K. Gray bars and black straight lines are guides for the eye, helping to visualize the slope changes at $T_d$ occurring in the 1$h$ sample of each series. Inset in (a): comparison between the $I_{\tau_R}(T)$ of PNIPAM 1$h$ collected on two different spectrometers.

the restricted $Q$ range 1.27−1.76 Å$^{-1}$, which is common to the two instruments.

≈

Inspection of $I_{\tau_R}(T)$ allows a first identification of $T_d$ by detection of the slope changes witnessing the activation of the sample dynamics. Although providing only a first qualitative indication, this evaluation has the advantage of being model independent. On comparing the behavior of PNIPAM, PNIPAM:d-glyc, and PNIPAM:d-glu at the highest hydration degree (1$h$), a slope change can be observed at $T_d$ in the temperature range between 220 and 240 K for all three systems, independently from the presence of cosolvents. Conversely, in the anhydrous samples (0$h$), the dynamical transition is strongly affected by the solvent composition: it is substantially suppressed in pure PNIPAM, whereas it occurs at ≈270 K in PNIPAM:d-glyc and at ≈370 K in PNIPAM:d-glu. In the other samples with cosolvents, at the intermediate hydration degrees between 0$h$ and 1$h$, increasing the water content $T_d$ progressively decreases from its value in the anhydrous sample to ≈230 K.

Further inspection of $I_{\tau_R}(T)$ reveals also the presence of additional slope changes besides $T_d$. In pure PNIPAM at 1$h$ (panel a), a drastic intensity decrease is observed at ≈270 K. The sharpness of the drop suggests the occurrence of a structural phase transition such as melting of $D_2O$ rather than a dynamical effect. Indeed, calorimetric studies on hydrated PNIPAM[67,68] and, in particular, recent investigations on $D_2O$-hydrated PNIPAM chains with the same molecular weight of those considered herein[69] showed that, in samples with $h$ = 1, a fraction of water molecules undergoes cold crystallization on heating and subsequently melts at ≈270 K. A smaller fraction of molecules undergoes crystallization upon cooling and melts at ≈277 K on heating with the total amount of crystalline water however being quite low.[69] In the context of hydrated polymers, cold crystallization is associated with "weakly-bound" water, i.e., a population of water molecules forming with polymer chains an interaction of intermediate strength between that of free bulk molecules, which crystallize upon cooling, and bound hydration molecules, which never crystallize.[70−72] Upon further heating such cold-crystallized molecules eventually melt, but the melting temperature is lower than that in the bulk because of the confining effect due to the interaction with polymer chains.[73,74] The intensity drop around 270 K in our PNIPAM 1$h$ sample can therefore be ascribed to the coupling of the polymer dynamics with melting of weakly bound water molecules. Above ≈275 K, when the phase transition is completed, the intensity slope goes back to a nearly constant linear trend. A similar effect is also observed in PNIPAM:d-glyc 1$h$ (Figure 2b) and PNIPAM:d-glu 1$h$ (Figure 2c), respectively, around 260 and 270 K, suggesting the occurrence of a structural phase transition also in these two samples.

Moving back to the low-temperature region, the data of pure PNIPAM (Figure 2a) show that $I_{\tau_R}(Q)$ for the dry sample is slightly but systematically lower than that for the hydrated one, indicating a higher rigidity of the hydrated polymer. Similar evidence is also found in proteins,[38,61,75] DNA,[76] and small peptides,[77] for which it has been suggested that at low temperatures frozen water reduces the MSDs of the macromolecule by constraining its fast fluctuations.

A last interesting observation arises from the comparison between values of $I_{\tau_R}(T)$ at different $\tau_R$. As reported in the inset of Figure 2a, in PNIPAM 1$h$ the overall intensity decrease as a function of $T$ is more pronounced for longer $\tau_R$ values,


https://doi.org/10.1021/acs.macromol.2c00177
Macromolecules 2022, 55, 4752−4765

Table 2. Values of $d$, $\phi$, $\xi$, $a$, and $C$ Obtained from the Fit on the Whole Data Set with the Corresponding Reduced $\chi^2$

| $\tau_R$ [ps] | $\xi$ | $\phi$ [Å/ps$^\xi$] | $d$ [Å] | $a$ [Å$^2$ × 10$^{-4}$/K] | $C$ [Å$^2$] | $\chi^2$ |
|---|---|---|---|---|---|---|
| 150 | 0.251 ± 0.003 | 0.361 ± 0.008 | 1.27 ± 0.03 | 1.95 ± 0.04 | 0.006 ± 0.002 | 3.2 |
| 2000 | | | 2.43 ± 0.06 | | | |

consistent with the fact that a larger fraction of moving atoms gets out of a smaller elastic window.

The qualitative picture emerging so far suggests a tight coupling between the dynamics of PNIPAM and that of the surrounding solvent. More quantitative information can be obtained from the analysis of the $Q$ dependence of the EINS intensities, as detailed in the following.

**3.2. Mean Square Displacements.** The MSDs of each sample, $\langle \Delta u^2 \rangle_{tot}$, were obtained by fitting the $Q$ dependence of the corresponding set of EINS intensities using the procedure reported in the Materials and Methods. As described in this section, the double-well distance $d$ was constrained to follow the behavior $d = \phi \tau_R^{\xi}$. The analysis provides the parameter values $\xi = 0.251 \pm 0.003$ and $\phi = (0.361 \pm 0.008)$ Å/ps$^\xi$ (see Table 2), with $\xi < 0.5$ indicating a subdiffusive motion.[64,66] The corresponding values of $d$ are 1.27 ± 0.03 Å at $\tau_R$ = 150 ps and 2.43 ± 0.06 Å at $\tau_R$ = 2000 ps. For comparison, several studies showed that the dynamical transition in proteins involves the activation of localized motions between ≈1.5 and ≈3 Å,[75,78] associated with large-amplitude backbone and side-chain fluctuations.[79,80] The role of backbone and side-chain dynamics in the dynamical transition has been highlighted also in PNIPAM microgels.[20]

The dynamical transition temperature $T_d$ of each sample was defined as the intersection between two straight lines obtained by fitting $\langle \Delta u^2 \rangle_{tot}$ in two temperature ranges, respectively, below and above the corresponding slope change. The resulting values of $T_d$ are reported in Table 3. In the following, we will separately analyze the MSDs of PNIPAM in each of the three investigated environments.

Table 3. Dynamical Transition Temperatures $T_d$ As Obtained from the Linear Fit of the MSDs

| | $T_d$ [K] | |
|---|---|---|
| sample | $\tau_R$ = 150 ps | $\tau_R$ = 2000 ps |
| PNIPAM 0$h$ | | |
| PNIPAM 1$h$ | 220 ± 2 | 220 ± 1 |
| PNIPAM:d-glyc 0$h$ | 270 ± 5 | 270 ± 1 |
| PNIPAM:d-glyc 0.15$h$ | 248 ± 6 | 248 ± 1 |
| PNIPAM:d-glyc 0.35$h$ | 225 ± 5 | 230 ± 2 |
| PNIPAM:d-glyc 1$h$ | 218 ± 4 | 219 ± 2 |
| PNIPAM:d-glu 0$h$ | 357 ± 2 | 380 ± 5 |
| PNIPAM:d-glu 0.15$h$ | 298 ± 6 | 301 ± 2 |
| PNIPAM:d-glu 0.35$h$ | 255 ± 5 | |
| PNIPAM:d-glu 1$h$ | 225 ± 11 | 234 ± 1 |

*3.2.1. Pure PNIPAM.* The MSDs of pure PNIPAM are reported in Figure 3. In agreement with the larger value assumed by $d$ at longer $\tau_R$, the resulting $\langle \Delta u^2 \rangle_{tot}$ are greater at $\tau_R$ = 2000 ps than at $\tau_R$ = 150 ps.

The MSDs of PNIPAM 0$h$ do not show abrupt changes in the slope, consistent with the fact that the dynamical transition is essentially suppressed when the system approaches dry conditions, as widely reported for various biomolecules[80,81] and, more recently, for PNIPAM microgels[21] and linear chains.[19] At low temperatures, a slight deviation of the MSDs

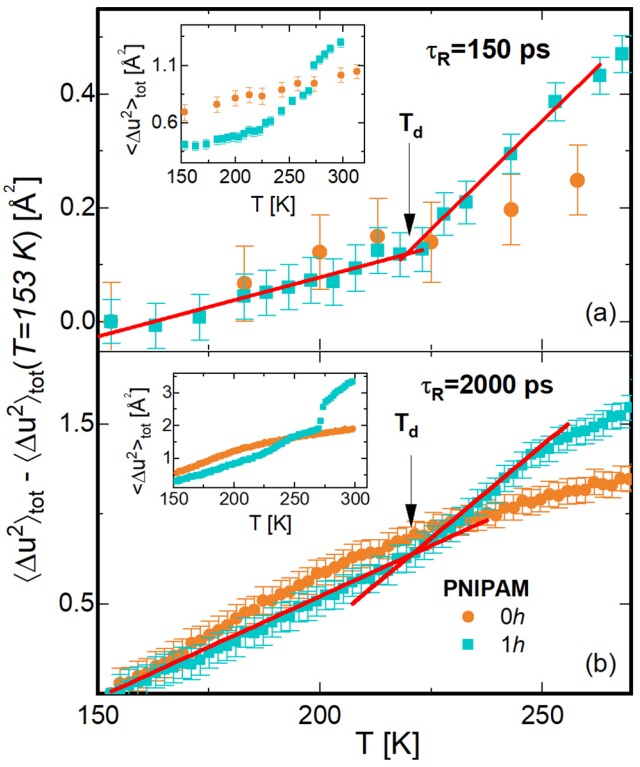


Figure 3. $\langle \Delta u^2 \rangle_{tot}$ of pure PNIPAM. For easier comparison of their slope, data were corrected for their value at 153 K (unsubtracted data are shown in the insets). Red lines result from the linear fit of $\langle \Delta u^2 \rangle_{tot}$ for the 1$h$ sample. Arrows indicate the slope change at $T_d$.

from a straight linear trend can be observed especially at $\tau_R$ = 2000 ps, as they smoothly inflect over a broad temperature range between ≈153 and ≈200 K. The behavior of the MSDs might be reminiscent of the activation of the rotational dynamics of methyl groups, typical of PNIPAM-based systems[20] as well as of other polymers and biological molecules.[25,47,80−82] Methyl dynamics becomes active between 100 and 150 K on the time scales accessible to neutron scattering, independent from the presence and composition of the solvent. Indeed, methyl rotations are characterized by a rather wide distribution of activation energies, yielding a distribution of activation temperatures which eventually results in a smeared MSDs response.[81,82] Considering this, we can infer that although the start of the methyl rotation processes occurs at temperatures lower than those investigated in this paper, the ending tail of methyl dynamics activation can still be observed in our temperature range.

In PNIPAM 1$h$, a dynamical transition clearly takes place at $T_d \approx 220$ K (see Table 3), similarly to hydrated biomolecules.[24,26,80,81] A close value of about 225 K has been previously reported for PNIPAM chains at 0.67$h$,[19] suggesting that $T_d$ remains substantially unaffected when the hydration level increases from 0.67$h$ to 1$h$. This allows one to separate the dynamical transition from the glass transition of hydrated PNIPAM, reported by calorimetric investigations.[67,69] Contrary to $T_d$, the glass transition temperature $T_g$


https://doi.org/10.1021/acs.macromol.2c00177
Macromolecules 2022, 55, 4752−4765

of PNIPAM shows a strong dependence on $h$, and in particular, it shifts from 243 K at 0.67$h$ to 230 K at 1$h$. A distinction between glass and dynamical transitions has also been pointed out for hydrated proteins, where the former is reflected in a mild slope change in the MSDs at $T_g \approx 200$ K followed by a more marked change at $T_d$ due to the dynamical transition.[28] However, the observation of the slope change at $T_g$ has proven elusive since in most cases it is hidden by the occurrence of the sharper dynamical transition.

At low temperatures, the MSDs of PNIPAM 1$h$ are smaller than those in the dry sample. As discussed for the corresponding EINS intensities, the decreased mobility of hydrated PNIPAM is probably caused by the constraining action exerted on the polymer by frozen water: since the layer of frozen water surrounding the polymer is stiffer than the polymer itself, also the water−PNIPAM mixture is on average stiffer and thus "more harmonic" than the polymer alone. In the same sample, the drastic jump of the MSDs at ≈270 K (see insets of Figure 3) is related to the fact that, on heating, some hydration water molecules cold crystallize and subsequently melt within a narrow temperature range around 270 K with consequent release of PNIPAM degrees of freedom.

*3.2.2. PNIPAM with Glycerol.* The MSDs of PNIPAM:d-glyc at $\tau_R$ = 150 and 2000 ps are shown in Figure 4a and 4b, respectively. Contrary to the case of pure PNIPAM, a dynamical transition occurs even in the absence of water (0$h$) at $T_d \approx 270$ K (see Table 3). On adding water, $T_d$ progressively shifts toward lower values, passing from ≈250 K at 0.15$h$ to ≈230 K at 0.35$h$ and ≈220 K at 1$h$.

Below $T_d$, for $\tau_R$ = 150 ps, a further and slight change in slope is observed in the 0$h$ and 0.15$h$ samples at $T_g = 206 \pm 7$ and 196 ± 10 K, respectively (see inset of Figure 4a). Identification of this slope change with the dynamical transition is unlikely because the presence of glycerol is expected to slow down the dynamics of PNIPAM, and therefore, $T_d$ should not occur below the value of ≈220 K found in pure water. Considering that the glass transition of the corresponding water/glycerol mixtures falls around 190 and 180 K, respectively,[83] the observed change may be related instead to a coupling with the solvent glass transition. This interpretation has been proposed to explain a similar slight change at ≈200 K in the MSDs of lysozyme in pure glycerol.[28]

Above $T_d$, closer inspection of the MSDs of PNIPAM:d-glyc 1$h$ reveals an additional slope increase at $T_{in} \approx 230$ K followed by a slope decrease at $T_m \approx 250$ K. To assess whether this behavior is related to a solvent phase transition as in the case of PNIPAM 1$h$, we performed calorimetric measurements on this sample (see Figure S5 of the Supporting Information). The thermogram shows a broad endothermic peak in the same temperature range, which is compatible with a progressive solvent melting process, starting at about $T_{in}$ and ending at $T_m$. The observation of a large peak is consistent with the fact that water/glycerol mixtures alone are rather polymorphic systems, where multiple and partially overlapping solid-state phase changes are observed.[84] Moreover, the interaction with PNIPAM can induce local fluctuations of the nominal solvent composition with a consequent distribution of melting temperatures, which can further explain the observed broadening of the melting peak. The MSDs behavior between $T_{in}$ and $T_m$ is well consistent with the calorimetric data and the progressive melting of such distributions of solid phases and/or solvent compositions.

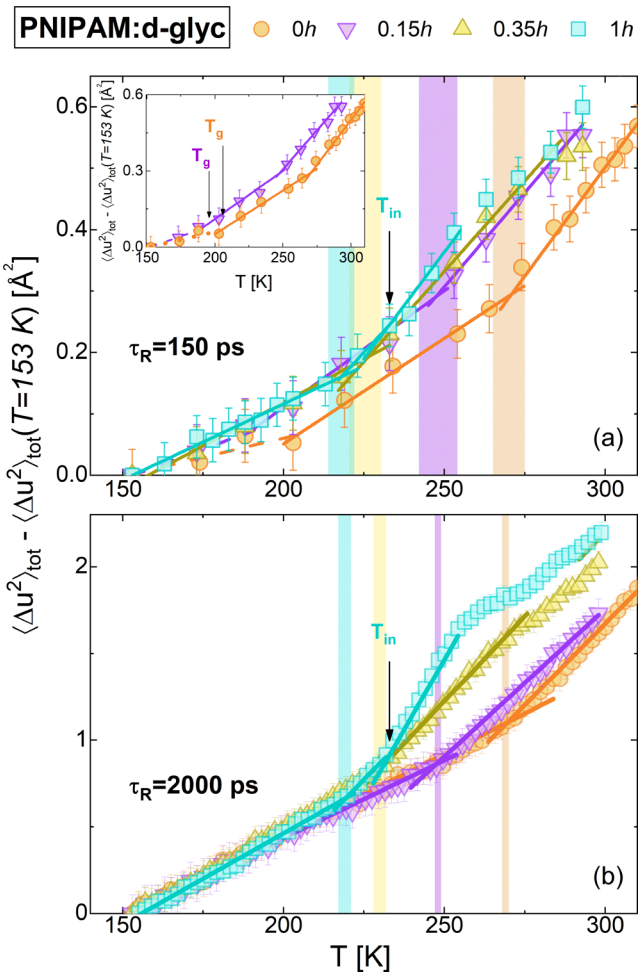


**Figure 4.** $\langle\Delta u^2\rangle_{tot}$ of PNIPAM:d-glyc at $\tau_R$ = 150 (a) and 2000 ps (b). MSDs are corrected for their value at $T$ = 153 K. Solid lines and colored bars help to visualize for each sample the slope changes at $T_d$. Further slope changes at $T_{in}$ are indicated by arrows. In the inset, slope changes at $T_g$ are highlighted.

*3.2.3. PNIPAM with Glucose.* The MSDs of PNIPAM:d-glu are shown in Figure 5. Compared to PNIPAM and PNIPAM:d-glyc, the slightly nonlinear trend at low temperatures that we attributed to methyl dynamics is now more pronounced, as especially evident at $\tau_R$ = 2000 ps (Figure 5b).

A dynamical transition is observed at all of the investigated $h$ values, and the corresponding $T_d$ values are reported in Table 3. In the anhydrous sample (0$h$), the transition occurs at very high temperatures for both time resolutions, namely, ≈360 K for $\tau_R$ = 150 ps and ≈380 K for $\tau_R$ = 2000 ps. In the latter case, a further and sudden increase of the MSDs appears above 400 K, close to the melting temperature of pure glucose. This suggests the formation of crystalline domains within an otherwise amorphous sample. Indeed, cold crystallization of amorphous glucose is observed roughly between 360 and 380 K in the presence of trace amounts of water followed by melting.[85] In this sample, cold crystallization of glucose might also explain the upshift of $T_d$ with respect to PNIPAM:d-glu 0$h$ measured at $\tau_R$ = 150 ps since the increased rigidity due to cold crystallization would compete with the increased mobility due to the dynamical transition, thus retarding to 380 K the observation of $T_d$.



https://doi.org/10.1021/acs.macromol.2c00177
Macromolecules 2022, 55, 4752−4765

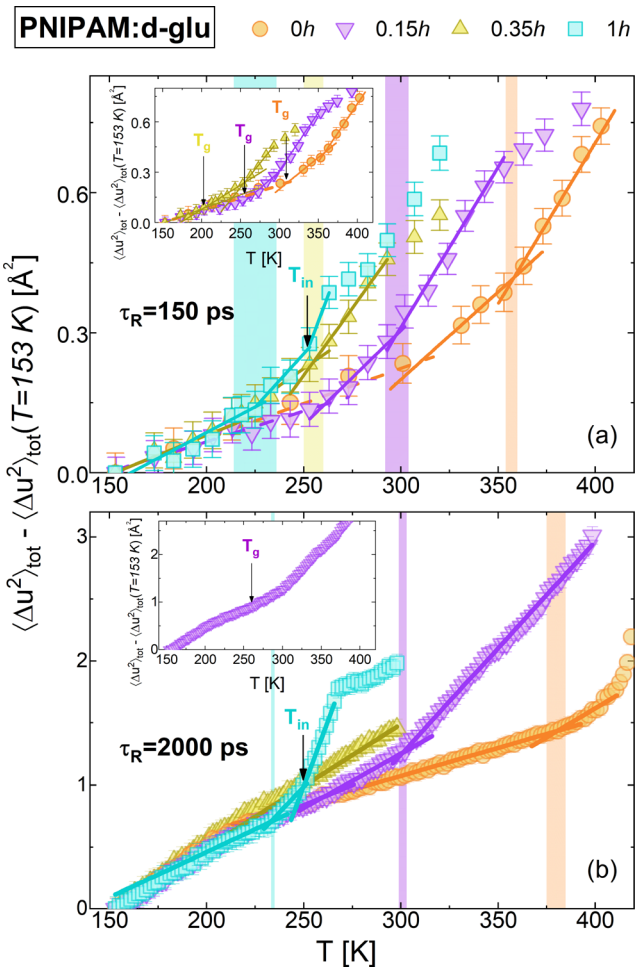


**Figure 5.** $\langle \Delta u^2 \rangle_{tot}$ of PNIPAM:d-glu at $\tau_R$ = 150 (a) and 2000 ps (b). MSDs are corrected for their value at $T$ = 153 K. Solid lines and colored bars help to visualize for each sample the slope changes at $T_d$. Further slope changes at $T_{in}$ are indicated by arrows. In the insets, the slope changes at $T_g$ are highlighted.

On increasing $h$, $T_d$ shifts to ≈300 K at 0.15$h$, ≈260 K at 0.35$h$, and ≈230 K at 1$h$. The PNIPAM:d-glu 0.35$h$ sample measured at $\tau_R$ = 2000 ps constitutes a peculiar case because the MSDs do not show any marked change in slope that can be associated with the dynamical transition. In fact, at this hydration level, $T_d$ gets close to the concomitant low-temperature inflection associated with methyl groups dynamics, which can thus prevent clear observation of the dynamical transition. In PNIPAM:d-glu 1$h$, the onset of the transition becomes visible again as a slope change despite the methyl contribution since the higher water content enhances the MSDs increase due to the activation of conformational dynamics.

Below $T_d$, a mild slope change is observed at $\tau_R$ = 150 ps in the 0$h$, 0.15$h$, and 0.35$h$ samples, respectively, at $T_g$ = 309 ± 7, 261 ± 6, and 202 ± 11 K (see the inset of Figure 5a). A slope change at $T_g$ = 260 ± 7 K is observed in PNIPAM:d-glu 0.15$h$ also at $\tau_R$ = 2000 ps (inset of Figure 5b). In analogy with the case of PNIPAM:d-glyc, this might be due to a coupling of the fast dynamics of PNIPAM with the glass transition of the solvent. By comparison, the glass transition temperature of the corresponding solvent mixture falls at about 300, 240, and 200 K, respectively.[86] A similar slope change at $T_g$ ≈ 300 K is observed also in the MSDs of lysozyme in pure glucose.[28]

In the MSDs of the 1$h$ sample, a further slope increase above $T_d$ is observed at $T_{in}$ ≈ 250 K followed by an abrupt slope decrease at $T_m$ ≈ 260 K. Similarly to the case of PNIPAM:d-glyc 1$h$, we interpret $T_{in}$ and $T_m$, respectively, as the starting and ending points of a solvent melting process, as confirmed by calorimetric data (see Figure S6 of the Supporting Information).

## 4. DISCUSSION

Overall, the above findings reveal a complex behavior of the PNIPAM atomic dynamics as a function of solvent composition, reflecting the complex interplay of microscopic interactions between PNIPAM and water, PNIPAM and cosolvent, and water and cosolvent. The most striking result is that in the presence of a cosolvent $T_d$ strongly depends on the hydration level $h$: as shown in Figure 6, on increasing water

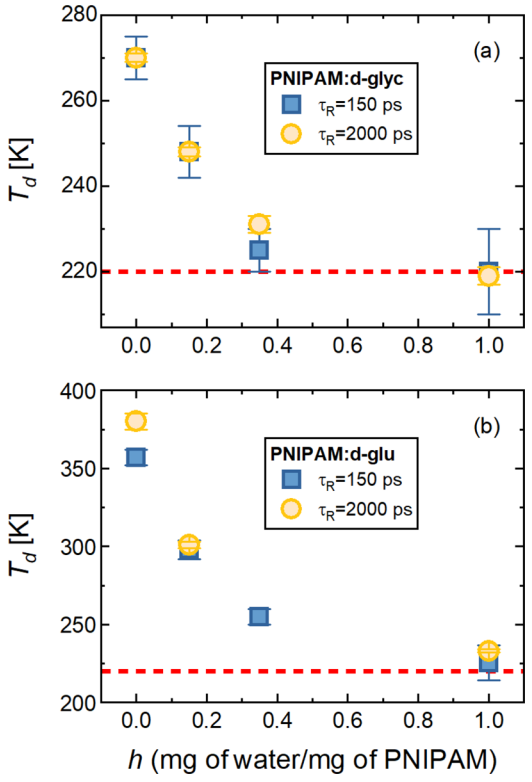


**Figure 6.** Dynamical transition temperatures $T_d$ of (a) PNIPAM:d-glyc and (b) PNIPAM:d-glu as a function of $h$. Dashed red lines indicate the value of $T_d$ in PNIPAM 1$h$ (without cosolvents).

content, $T_d$ tends to its value without cosolvents and reaches it already at 1$h$. In light of this, it is convenient to discuss our results by separating those obtained in the high-hydration regime ($h \approx 1$) from those in the low-hydration regime ($h \lesssim 0.4$). In the high-hydration regime, water-mediated interactions are predominant, as suggested by the fact that $T_d$ behaves as if the cosolvent were not present. In the low-hydration regime instead, where $T_d$ strongly depends on the solvent composition, we expect PNIPAM−cosolvent interactions to be more effective.

**4.1. High-Hydration Regime.** In PNIPAM−water−cosolvent samples at 1$h$, the value of $T_d$ is close to that found in the PNIPAM−water sample without cosolvent (Figure 6). This suggests that in ternary samples when the hydration level is sufficiently high, cosolvent molecules tend to


https://doi.org/10.1021/acs.macromol.2c00177
Macromolecules 2022, 55, 4752−4765

be preferentially excluded from the PNIPAM solvation shell with the polymer being therefore preferentially hydrated. Such a mechanism of preferential hydration has already been proposed for the interaction between sugars and PNIPAM in diluted solutions.[12,87] Recent investigations, in particular, showed how the addition of a sugar (trehalose) to aqueous PNIPAM results in a preferential exclusion of the cosolvent from the polymer surface, with the sugar developing strong interactions with water molecules while the polymer hydration state is preserved.[12] Our results extend the preferential exclusion mechanism to much more concentrated PNIPAM dispersions as well as to the case of a polyol cosolvent like glycerol.

Preferential exclusion of stabilizing compounds is observed also in aqueous solutions of proteins.[88−90] In particular, an $h$ dependence of $T_d$ similar to that shown in Figure 6 has been observed for lysozyme embedded in water/glycerol and water/glucose matrices, where $T_d$ reaches its limiting value for $h \gtrsim 0.4$.[43−45] On comparing the two systems, it seems that preferential exclusion starts to take place at similar values of $h$ in both PNIPAM and lysozyme, which suggests that PNIPAM linear chains have a capability to coordinate and confine water molecules comparable to proteins. This is likely an essential requisite for the "biomimic" character of PNIPAM, especially considering that it is precisely this kind of confined, proximal water that plays a major role in determining protein functional dynamics.[23]

From the MSDs, an estimate of the polymer rigidity can be obtained by means of the pseudoforce constant[91] $k = 0.00276/\left(\frac{d\langle \Delta u^2\rangle_{tot}}{dT}\right)$, where $k$ is expressed in N/m if $\langle \Delta u^2\rangle_{tot}$ is given in Å$^2$ and $T$ in K. In general, we expect $k$ to depend on both the solvent composition and the temperature since it will be influenced by the activation of anharmonic processes and by phase transitions. By looking at the MSDs reported in Figure 7, three different temperature regions to calculate $k$ can be identified in each sample: (1) a low-temperature region, below the dynamical transition temperature $T_d$; (2) an intermediate-temperature region, above $T_d$ and below the start of solvent melting at $T_{in}$; (3) a high-temperature region above $T_m$, where the melting transition is completed.

In the low-temperature region, where only harmonic and methyl dynamics are active, the MSDs are small, indicating low flexibility, and the associated pseudoforce constants are rather large, as shown in Figure 8. A larger $k$ is observed in the presence of cosolvents, especially in the case of glucose and for $\tau_R$ = 2000 ps, where the data have better statistics and a finer temperature sampling.

In the intermediate-temperature region, the occurrence of the dynamical transition leads to an increase of the MSDs slope in all samples, and a corresponding decrease of $k$ is observed for both of the investigated $\tau_R$ values. As in the previous case, higher values of $k$ are found in the presence of cosolvents and the effect is larger for glucose. The stronger constraining action of glucose on the dynamics of PNIPAM is also witnessed by the fact that it shifts $T_d$ to a value about 10 K higher than in the other two hydrated samples.

In the high-temperature region, the presence of cosolvents is particularly influential in determining the value of $k$. On one hand, in the purely hydrated sample, the pseudoforce constant decreases from the values assumed in the low- and intermediate-temperature regions at both $\tau_R$ values. On the other hand, in the presence of cosolvents, $k$ increases, indicating that the polymer becomes more rigid than in the intermediate-temperature regime, as especially evident at $\tau_R$ = 2000 ps. Such a reduced mobility of PNIPAM at high temperature might be explained by a temperature effect on the preferential hydration mechanism. Indeed, preferential hydration in these samples should lead to the presence of a water-rich environment around the polymer, which, below melting, might allow PNIPAM to be relatively flexible. Above melting, solvent molecules diffuse more freely; therefore, preferential hydration might become less effective and PNIPAM might sense a more homogeneous and viscous environment. A further contribution to the increased polymer rigidity at high temperature can derive from the transition of PNIPAM to the more compact globular conformation above the LCST, as mentioned in the Supporting Information. It is worth noting that recent computational investigations on the PNIPAM−water−trehalose system at $T$ = 283 and 318 K showed how preferential exclusion of trehalose from the PNIPAM solvation shell is less effective at the highest investigated temperature (when the polymer is in the globule conformation).[12]

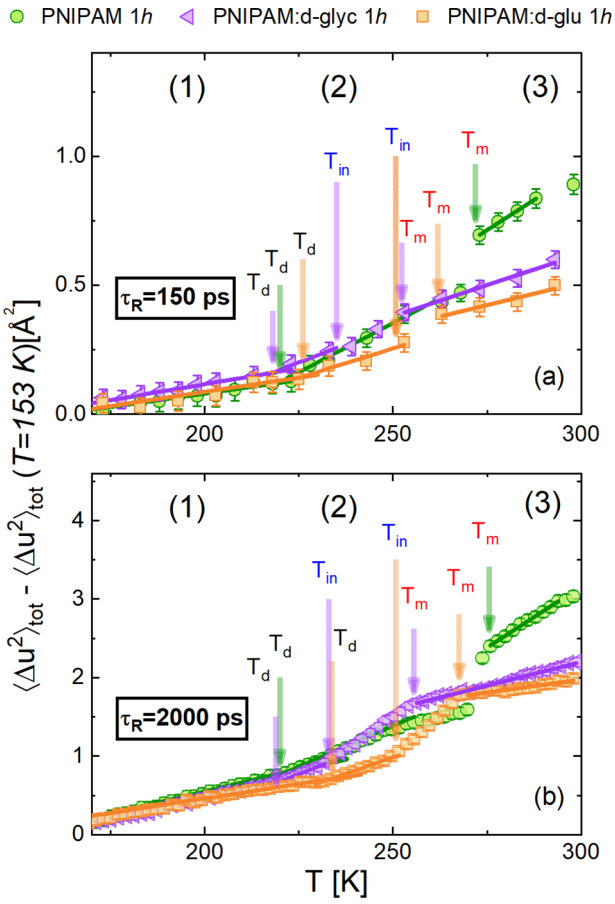


**Figure 7.** MSDs of PNIPAM, PNIPAM:d-glyc, and PNIPAM:d-glu in the high-hydration regime (1$h$). MSDs are corrected for the corresponding value at $T$ = 153 K. For each sample, the corresponding values of $T_d$, $T_{in}$, and $T_m$ are indicated by arrows. Solid lines are obtained from the linear fit of the data in the temperature region below $T_d$ (1), above $T_d$ and below $T_{in}$ (2), and above $T_m$ (3).

**4.2. Low-Hydration Regime.** We will now examine the behavior of the MSDs of PNIPAM samples in the anhydrous state (0$h$) reported in Figure 9. At low temperatures, the



https://doi.org/10.1021/acs.macromol.2c00177
Macromolecules 2022, 55, 4752−4765

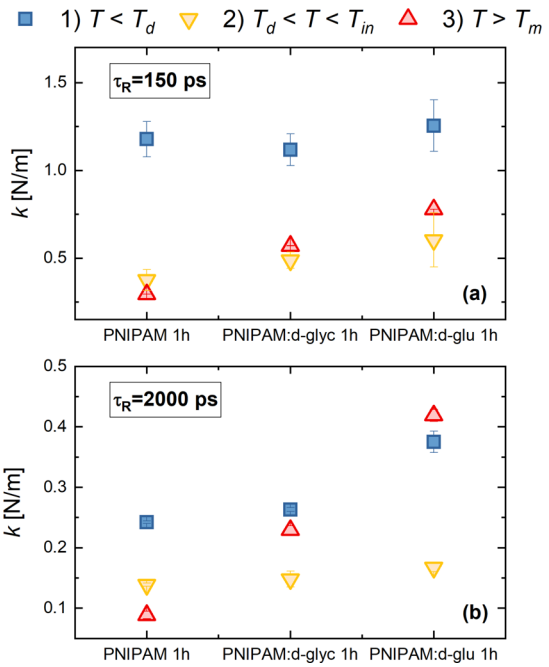


**Figure 8.** Pseudoforce constant $k$ at $\tau_R$ = (a) 150 and (b) 2000 ps calculated for PNIPAM samples at 1$h$. Values of $k$ are obtained from the MSDs slope in the temperature region (1) below $T_d$ (red), (2) between $T_d$ and $T_{in}$ (blue), and (3) above $T_m$ (yellow).

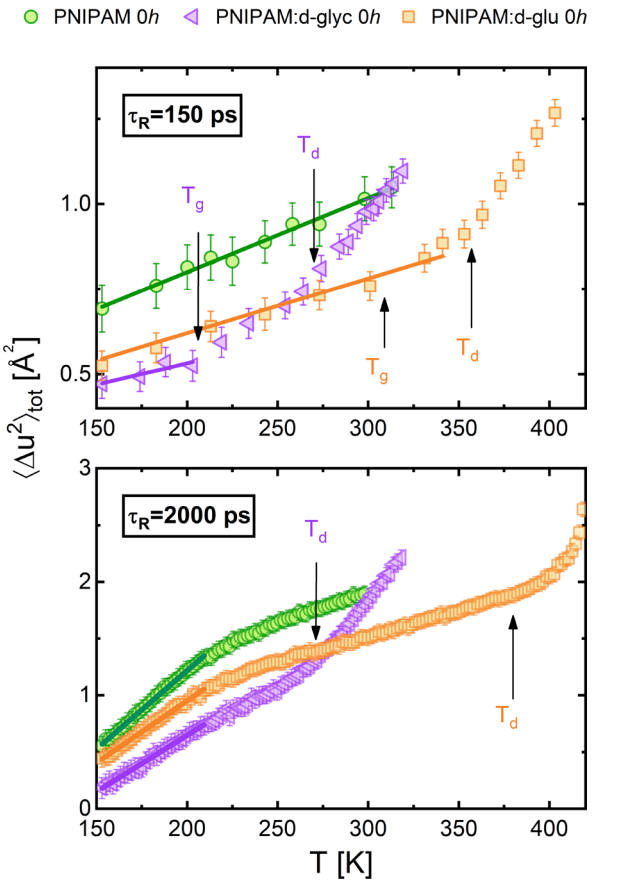


**Figure 9.** MSDs of PNIPAM, PNIPAM:d-glyc, and PNIPAM:d-glu at the same hydration degree (0$h$). For each binary sample, the corresponding values of $T_d$ and $T_g$ are indicated by arrows. Solid lines are obtained from the linear fit of the MSDs in the temperature range between 153 and 313 K, 153 and 203 K, 153 and 303 K, respectively, for PNIPAM, PNIPAM:d-glyc, and PNIPAM:d-glu at $\tau_R$ = 150 ps. All MSDs were fitted in the same temperature range between 153 and 209 K at $\tau_R$ = 2000 ps.

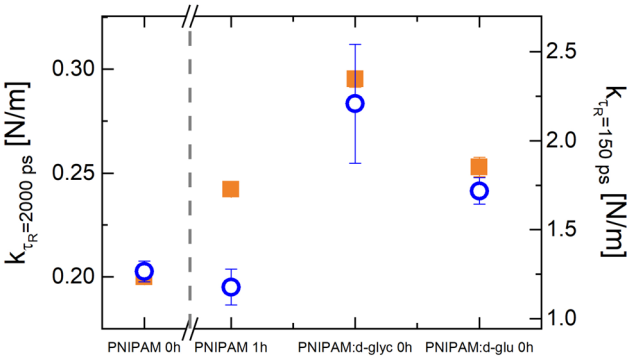


**Figure 10.** Low-temperature pseudoforce constant $k$ at $\tau_R$ = 150 (empty circles) and 2000 ps (solid squares) calculated for dry PNIPAM (0$h$) compared with values calculated for PNIPAM embedded in pure water (PNIPAM 1$h$), pure glycerol (PNIPAM:d-glyc 0$h$), and pure glucose (PNIPAM:d-glu 0$h$).

MSDs of pure PNIPAM are larger than those of PNIPAM embedded in glycerol and glucose. Correspondingly, the pseudoforce constants $k$ are smaller in pure PNIPAM than those in glycerol or glucose (Figure 10). As a whole, both the MSDs and the $k$ values indicate a higher mobility of the pure polymer with respect to PNIPAM embedded in glycerol or glucose. We already observed an analogous behavior for PNIPAM in water alone at 1$h$, where the MSDs below $T_d$ are smaller than those in the dry sample (see Figure 3), and we ascribed this effect to the constraining action exerted by frozen water. We can now conclude that below $T_d$ the addition of any of the three investigated solvents results in a stiffening of the polymer, irrespective of the specific nature of the solvent. However, the constraining action of the two cosolvents, and especially of glycerol, in particular, appears more effective than that of water, since the pseudoforce constant $k$ is smaller in PNIPAM 1$h$ than in PNIPAM:d-glyc 0$h$ and PNIPAM:d-glu 0$h$ (see Figure 10). A similar low-temperature antiplasticizing effect of glycerol is observed in proteins, where the increase of rigidity is ascribed to a greater ability of this cosolvent to stabilize the surface moieties compared to water.[92] Antiplasticization of fast motions at low temperatures is especially relevant in the protein context, since it is thought to inhibit protein degradation and thus favor stabilization.[93]

A crossover from an antiplasticizing to a plasticizing effect of glycerol is observed on increasing the temperature well above $T_d \approx 270$ K with the MSDs of pure PNIPAM becoming progressively smaller than those of PNIPAM:d-glyc. Such a crossover has also been observed in the MSDs of lysozyme embedded in glycerol.[48,94] An extrapolation of the data reported in Figure 9 suggests that a similar crossover might also occur in PNIPAM:d-glu above the corresponding $T_d \approx$ 370 K, although data for pure PNIPAM at such high temperatures were not collected.

In PNIPAM:d-glyc and PNIPAM:d-glu, the absence of water and the consequent shift of $T_d$ toward higher values allow the observation of an additional small change of slope at $T_g < T_d$. As mentioned above, such a low-temperature change in proteins is ascribed to a coupling of the biomolecule dynamics


https://doi.org/10.1021/acs.macromol.2c00177
Macromolecules 2022, 55, 4752−4765

with the slow $\alpha$ relaxation and hence the glass transition of the surrounding solvent.[28] A similar slope change should be observed also in hydrated samples. In the latter case, however, the proximity of $T_g$ to $T_d$ often does not allow one to clearly separate the two processes.

The dynamical transition instead, which occurs at higher temperatures, is not expected to be coupled with the slow $\alpha$ relaxation of the solvent. On the other hand, for a given solvent, the dynamical transition occurs around the same temperature for PNIPAM, proteins, and DNA:[25,28,45,48,95] for all of these macromolecules, $T_d$ falls around 220 K in water, 270 K in glycerol, and 370 K in glucose. This observation strongly supports the idea that also the dynamical transition is a solvent-driven process. Indeed, the most recent interpretations ascribe the dynamical transition to the fast $\beta$ relaxation of the solvent, whose characteristic time $\tau_\beta$ matches the typical instrumental resolutions of neutron backscattering spectrometers.[28,29] In this regard, it should be noted that since $\tau_\beta$ decreases with increasing temperature, an upshift of $T_d$ should be expected on decreasing $\tau_R$.[28] However, no appreciable dependence of $T_d$ on $\tau_R$ can be unambiguously detected in our set of data. The observation of such an effect might actually be prevented by specific experimental issues, such as the sparse temperature sampling at $\tau_R$ = 150 ps, as well as the superposition of several dynamical processes over the same temperature window. Future investigations are therefore needed to deepen this interesting aspect by means of a wider and more systematic sampling of the dynamical transition in PNIPAM as a function of the instrumental resolution.

## 5. CONCLUSIONS

Similarly to what was observed in biological polymers, the dynamical transition occurring in PNIPAM is critically affected by the solvent environment. The stabilizing character of glycerol and glucose is reflected by the fact that their addition to nonhydrated PNIPAM causes a shift of $T_d$ to higher values compared to the purely hydrated sample. This implies that the low-temperature constraining (antiplasticizing) action exerted by these compounds extends over a wider temperature range with respect to water.

When water is added, on increasing hydration level, the behavior of the system progressively shifts toward that of hydrated PNIPAM without cosolvents. This might indicate that a preferential exclusion of the cosolvent takes place when the system reaches a proper hydration level. This evidence confirms the hypothesis that the mechanism of interaction between PNIPAM and stabilizers in an aqueous environment is mainly water mediated.

Most of the distinctive features of the dynamical transition of biomolecules, including the transition temperature values, are replicated in PNIPAM. Overall, the existence of such strong analogies leads to two remarkable considerations. On one hand, they underline the prominent role of the solvent in the dynamical transition, which exhibits some universal features irrespective of the specific characteristics of the solvated macromolecule. On the other hand, they bear witness to the existence of fundamental mechanisms of solvent−solute interaction that are common to PNIPAM and biomacromolecules. From an essential point of view, the rich phenomenology of proteins in solution can be traced back to the subtle balance between the interactions of the protein polar and nonpolar groups, both among themselves and with solvent molecules, which ultimately leads to the complex biological behavior and functionality of proteins. Therefore, it may be argued that the ability of PNIPAM to replicate protein behavior is intimately connected to the intrinsic complexity of the polymer repeating unit, enabling it to reproduce the rich energy landscape of proteins with a multitude of different conformational substates. Future works may benefit from such unique properties of PNIPAM-based systems with the aim to extend their applications as artificial analogues of natural biomolecules.

## ■ ASSOCIATED CONTENT

### Supporting Information

The Supporting Information is available free of charge at https://pubs.acs.org/doi/10.1021/acs.macromol.2c00177.

Further details about the fitting strategy; differential scanning calorimetry analysis; comparison between neutron scattering and calorimetric data (PDF)

## ■ AUTHOR INFORMATION


### Corresponding Author

**Andrea Orecchini** − *Dipartimento di Fisica e Geologia, Università di Perugia, 06123 Perugia, Italy; Dipartimento di Fisica e Geologia, CNR-IOM c/o Università di Perugia, 06123 Perugia, Italy*; Email: andrea.orecchini@unipg.it

### Authors

**Benedetta P. Rosi** − *Dipartimento di Fisica e Geologia, Università di Perugia, 06123 Perugia, Italy*; orcid.org/0000-0001-9745-5826

**Arianna D'Angelo** − *Laboratoire de Physique des Solides, CNRS, Université Paris-Saclay, 91405 Orsay, France; Institut Laue-Langevin, 38042 Grenoble, Cedex 9, France*

**Elena Buratti** − *Dipartimento di Fisica, CNR-ISC c/o Università di Roma La Sapienza, 00185 Roma, Italy*; orcid.org/0000-0003-3982-5141

**Marco Zanatta** − *Dipartimento di Fisica, Università di Trento, 38123 Trento, Italy*

**Letizia Tavagnacco** − *Dipartimento di Fisica, CNR-ISC c/o Università di Roma La Sapienza, 00185 Roma, Italy*; orcid.org/0000-0002-3492-7766

**Francesca Natali** − *Institut Laue-Langevin, 38042 Grenoble, Cedex 9, France; CNR-IOM, OGG, 38043 Grenoble, Cedex 9, France*

**Michaela Zamponi** − *Jülich Centre for Neutron Science at Heinz Maier-Leibnitz Zentrum, Forschungszentrum Jülich GmbH, 85747 Garching, Germany*

**Daria Noferini** − *Jülich Centre for Neutron Science at Heinz Maier-Leibnitz Zentrum, Forschungszentrum Jülich GmbH, 85747 Garching, Germany; European Spallation Source ERIC, 221 00 Lund, Sweden*

**Silvia Corezzi** − *Dipartimento di Fisica e Geologia, Università di Perugia, 06123 Perugia, Italy*

**Emanuela Zaccarelli** − *Dipartimento di Fisica, CNR-ISC c/o Università di Roma La Sapienza, 00185 Roma, Italy*

**Lucia Comez** − *Dipartimento di Fisica e Geologia, CNR-IOM c/o Università di Perugia, 06123 Perugia, Italy*; orcid.org/0000-0001-5160-6844

**Francesco Sacchetti** − *Dipartimento di Fisica e Geologia, Università di Perugia, 06123 Perugia, Italy*

**Alessandro Paciaroni** − *Dipartimento di Fisica e Geologia, Università di Perugia, 06123 Perugia, Italy*




https://doi.org/10.1021/acs.macromol.2c00177
Macromolecules 2022, 55, 4752−4765

**Caterina Petrillo** − *Dipartimento di Fisica e Geologia, Università di Perugia, 06123 Perugia, Italy*

Complete contact information is available at: https://pubs.acs.org/10.1021/acs.macromol.2c00177

### Notes

The authors declare no competing financial interest.

## ■ ACKNOWLEDGMENTS

This publication was supported by the CarESS project, D.R. no. 597, from the University of Perugia. The authors acknowledge the Institut Laue-Langevin (ILL) and the Jülich Centre for Neutron Science (JCNS) at the Heinz Maier-Leibnitz Zentrum (MLZ) for beamtime allocation.

## ■ REFERENCES

(1) Aguilar, M. R.; San Román, J. *Smart Polymers and their Applications*, 2nd ed.; Woodhead Publishing, 2019; pp 1−11; DOI: 10.1016/B978-0-08-102416-4.00001-6.
(2) Schild, H. Poly(N-isopropylacrylamide): experiment, theory and application. *Prog. Polym. Sci.* **1992**, *17*, 163−249.
(3) Lim, H.; Hwang, Y.; Kar, M.; Varghese, S. Smart hydrogels as functional biomimetic systems. *Biomaterials Science* **2014**, *2*, 603−618.
(4) Alarcón, C. d. l. H.; Pennadam, S.; Alexander, C. Stimuli responsive polymers for biomedical applications. *Chem. Soc. Rev.* **2005**, *34*, 276−285.
(5) Guan, Y.; Zhang, Y. PNIPAM microgels for biomedical applications: From dispersed particles to 3D assemblies. *Soft Matter* **2011**, *7*, 6375−6384.
(6) Sun, T.; Qing, G. Biomimetic Smart Interface Materials for Biological Applications. *Adv. Mater.* **2011**, *23*, H57−H77.
(7) Inoue, M.; Hayashi, T.; Hikiri, S.; Ikeguchi, M.; Kinoshita, M. Comparison based on statistical thermodynamics between globule-to-coil transition of poly(N-isopropylacrylamide) and cold denaturation of a protein. *J. Mol. Liq.* **2020**, *317*, 114129.
(8) Inoue, M.; Hayashi, T.; Hikiri, S.; Ikeguchi, M.; Kinoshita, M. Mechanism of globule-to-coil transition of poly(N-isopropylacrylamide) in water: Relevance to cold denaturation of a protein. *J. Mol. Liq.* **2019**, *292*, 111374.
(9) Graziano, G. On the temperature-induced coil to globule transition of poly-N-isopropylacrylamide in dilute aqueous solutions. *Int. J. Biol. Macromol.* **2000**, *27*, 89−97.
(10) Tiktopulo, E. I.; Uversky, V. N.; Lushchik, V. B.; Klenin, S. I.; Bychkova, V. E.; Ptitsyn, O. B. Domain" Coil-Globule Transition in Homopolymers. *Macromolecules* **1995**, *28*, 7519−7524.
(11) Fujishige, S.; Kubota, K.; Ando, I. Phase transition of aqueous solutions of poly(N-isopropylacrylamide) and poly(N-isopropylmethacrylamide). *J. Phys. Chem.* **1989**, *93*, 3311−3313.
(12) Rosi, B. P.; Tavagnacco, L.; Comez, L.; Sassi, P.; Ricci, M.; Buratti, E.; Bertoldo, M.; Petrillo, C.; Zaccarelli, E.; Chiessi, E.; Corezzi, S. Thermoresponsivity of poly(N-isopropylacrylamide) microgels in water-trehalose solution and its relation to protein behavior. *J. Colloid Interface Sci.* **2021**, *604*, 705−718.
(13) Yan, X.; Chu, Y.; Liu, B.; Ru, G.; Di, Y.; Feng, J. Dynamic Mechanism of Halide Salts on the Phase Transition of Protein Models Poly(N-isopropylacrylamide) and Poly(N,N-diethylacrylamide). *Phys. Chem. Chem. Phys.* **2020**, *22*, 12644−12650.
(14) Zhang, Y.; Furyk, S.; Bergbreiter, D. E.; Cremer, P. S. Specific Ion Effects on the Water Solubility of Macromolecules: PNIPAM and the Hofmeister Series. *J. Am. Chem. Soc.* **2005**, *127*, 14505−14510.
(15) Wu, J.; Wang, X.; Wang, Q.; Lou, Z.; Li, S.; Zhu, Y.; Qin, L.; Wei, H. Nanomaterials with enzyme-like characteristics (nanozymes): next-generation artificial enzymes (II). *Chem. Soc. Rev.* **2019**, *48*, 1004−1076.
(16) Xie, J.; Zhang, X.; Wang, H.; Zheng, H.; Huang, Y.; Xie, J. Analytical and environmental applications of nanoparticles as enzyme mimetics. *Trends in Analytical Chemistry* **2012**, *39*, 114−129.
(17) Vial, L.; Dumy, P. Artificial enzyme-based biosensors. *New J. Chem.* **2009**, *33*, 939−946.
(18) Halperin, A.; Kröger, M.; Winnik, F. M. Poly(N-isopropylacrylamide) Phase Diagrams: Fifty Years of Research. *Angew. Chem., Int. Ed.* **2015**, *54*, 15342−15367.
(19) Tavagnacco, L.; Zanatta, M.; Buratti, E.; Rosi, B.; Frick, B.; Natali, F.; Ollivier, J.; Chiessi, E.; Bertoldo, M.; Zaccarelli, E.; Orecchini, A. Proteinlike dynamical transition of hydrated polymer chains. *Physical Review Research* **2021**, *3*, 013191.
(20) Tavagnacco, L.; Chiessi, E.; Zanatta, M.; Orecchini, A.; Zaccarelli, E. Water−Polymer Coupling Induces a Dynamical Transition in Microgels. *J. Phys. Chem. Lett.* **2019**, *10*, 870−876.
(21) Zanatta, M.; Tavagnacco, L.; Buratti, E.; Bertoldo, M.; Natali, F.; Chiessi, E.; Orecchini, A.; Zaccarelli, E. Evidence of a low-temperature dynamical transition in concentrated microgels. *Science Advances* **2018**, *4*, No. eaat5895.
(22) Doster, W.; Cusack, S.; Petry, W. Dynamical Transition of Myoglobin Revealed by Inelastic Neutron Scattering. *Nature* **1989**, *337*, 754−6.
(23) Schiró, G.; Weik, M. Role of hydration water in the onset of protein structural dynamics. *J. Phys.: Condens. Matter* **2019**, *31*, 463002.
(24) Cornicchi, E.; Capponi, S.; Marconi, M.; Onori, G.; Paciaroni, A. Temperature dependence of fast fluctuations in single- and double-stranded DNA molecules: a neutron scattering investigation. *Philos. Mag.* **2007**, *87*, 509−515.
(25) Cornicchi, E.; De Francesco, A.; Marconi, M.; Onori, G.; Paciaroni, A. A relationship between solvent viscosity and biomolecule picosecond thermal fluctuations. *Chem. Phys.* **2008**, *345*, 219−223.
(26) Caliskan, G.; Briber, R. M.; Thirumalai, D.; García-Sakai, V.; Woodson, S. A.; Sokolov, A. P. Dynamic Transition in tRNA is Solvent Induced. *J. Am. Chem. Soc.* **2006**, *128*, 32−33.
(27) Roh, J.; Briber, R.; Damjanovic, A.; Thirumalai, D.; Woodson, S.; Sokolov, A. Dynamics of tRNA at Different Levels of Hydration. *Biophys. J.* **2009**, *96*, 2755−2762.
(28) Capaccioli, S.; Ngai, K. L.; Ancherbak, S.; Paciaroni, A. Evidence of Coexistence of Change of Caged Dynamics at $T_g$ and the Dynamic Transition at $T_d$ in Solvated Proteins. *J. Phys. Chem. B* **2012**, *116*, 1745−1757.
(29) Ngai, K.; Capaccioli, S.; Paciaroni, A. Dynamics of hydrated proteins and bio-protectants: Caged dynamics, $\beta$-relaxation, and $\alpha$-relaxation. *Biochimica et Biophysica Acta (BBA) - General Subjects* **2017**, *1861*, 3553−3563.
(30) Chen, S.-H.; Liu, L.; Fratini, E.; Baglioni, P.; Faraone, A.; Mamontov, E. Observation of fragile-to-strong dynamic crossover in protein hydration water. *Proc. Natl. Acad. Sci. U. S. A.* **2006**, *103*, 9012−9016.
(31) Wood, K.; Frölich, A.; Paciaroni, A.; Moulin, M.; Härtlein, M.; Zaccai, G.; Tobias, D. J.; Weik, M. Coincidence of Dynamical Transitions in a Soluble Protein and Its Hydration Water: Direct Measurements by Neutron Scattering and MD Simulations. *J. Am. Chem. Soc.* **2008**, *130*, 4586−4587.
(32) Schiró, G.; Vetri, V.; Frick, B.; Militello, V.; Leone, M.; Cupane, A. Neutron Scattering Reveals Enhanced Protein Dynamics in Concanavalin A Amyloid Fibrils. *J. Phys. Chem. Lett.* **2012**, *3*, 992−996.
(33) Schiró, G.; Caronna, C.; Natali, F.; Koza, M. M.; Cupane, A. The "Protein Dynamical Transition" Does Not Require the Protein Polypeptide Chain. *J. Phys. Chem. Lett.* **2011**, *2*, 2275−2279.
(34) Niessen, K. A.; Xu, M.; Paciaroni, A.; Orecchini, A.; Snell, E. H.; Markelz, A. G. Moving in the Right Direction: Protein Vibrations Steering Function. *Biophys. J.* **2017**, *112*, 933−942.
(35) Henzler-Wildman, K.; Kern, D. Dynamic personalities of proteins. *Nature* **2007**, *450*, 964−972.
(36) Fenimore, P. W.; Frauenfelder, H.; McMahon, B. H.; Young, R. D. Bulk-solvent and hydration-shell fluctuations, similar to $\alpha$- and $\beta$-fluctuations in glasses, control protein motions and functions. *Proc. Natl. Acad. Sci. U. S. A.* **2004**, *101*, 14408−14413.

(37) Rasmussen, B. F.; Stock, A. M.; Ringe, D.; Petsko, G. A. Crystalline Ribonuclease A Loses Function Below the Dynamical Transition at 220 K. *Nature* **1992**, *357*, 423−424.
(38) Réat, V.; Patzelt, H.; Ferrand, M.; Pfister, C.; Oesterhelt, D.; Zaccai, G. Dynamics of different functional parts of bacteriorhodopsin: H-2H labeling and neutron scattering. *Proc. Natl. Acad. Sci. U. S. A.* **1998**, *95*, 4970−4975.
(39) Mensink, M. A.; Frijlink, H. W.; van der Voort Maarschalk, K.; Hinrichs, W. L. How sugars protect proteins in the solid state and during drying (review): Mechanisms of stabilization in relation to stress conditions. *Eur. J. Pharm. Biopharm.* **2017**, *114*, 288−295.
(40) Cicerone, M. T.; Pikal, M. J.; Qian, K. K. Stabilization of proteins in solid form. *Adv. Drug Delivery Rev.* **2015**, *93*, 14−24.
(41) Manning, M.; Chou, D.; Murphy, B.; Payne, R.; Katayama, D. Stability of Protein Pharmaceuticals: An Update. *Pharm. Res.* **2010**, *27*, 544−575.
(42) Cordone, L.; Ferrand, M.; Vitrano, E.; Zaccai, G. Harmonic Behavior of Trehalose-Coated Carbon-Monoxy-Myoglobin at High Temperature. *Biophys. J.* **1999**, *76*, 1043−1047.
(43) Cornicchi, E.; Marconi, M.; Onori, G.; Paciaroni, A. Controlling the Protein Dynamical Transition with Sugar-Based Bioprotectant Matrices: A Neutron Scattering Study. *Biophys. J.* **2006**, *91*, 289−297.
(44) Paciaroni, A.; Cinelli, S.; Onori, G. Effect of the Environment on the Protein Dynamical Transition: A Neutron Scattering Study. *Biophys. J.* **2002**, *83*, 1157−1164.
(45) Katava, M.; Stirnemann, G.; Zanatta, M.; Capaccioli, S.; Pachetti, M.; Ngai, K. L.; Sterpone, F.; Paciaroni, A. Critical structural fluctuations of proteins upon thermal unfolding challenge the Lindemann criterion. *Proc. Natl. Acad. Sci. U. S. A.* **2017**, *114*, 9361−9366.
(46) Marconi, M.; De Francesco, A.; Cornicchi, E.; Onori, G.; Paciaroni, A. Hydration and temperature dependent dynamics of lysozyme in glucose−water matrices. A neutron scattering study. *Chem. Phys.* **2005**, *317*, 274−281.
(47) Paciaroni, A.; Cornicchi, E.; De Francesco, A.; Marconi, M.; Onori, G. Conditioning action of the environment on the protein dynamics studied through elastic neutron scattering. *Eur. Biophys. J.* **2006**, *35*, 591−599.
(48) Tsai, A. M.; Neumann, D. A.; Bell, L. N. Molecular Dynamics of Solid-State Lysozyme as Affected by Glycerol and Water: A Neutron Scattering Study. *Biophys. J.* **2000**, *79*, 2728−2732.
(49) Tsai, A. M.; Udovic, T. J.; Neumann, D. A. The Inverse Relationship between Protein Dynamics and Thermal Stability. *Biophys. J.* **2001**, *81*, 2339−2343.
(50) Weng, L.; Stott, S. L.; Toner, M. Exploring Dynamics and Structure of Biomolecules, Cryoprotectants, and Water Using Molecular Dynamics Simulations: Implications for Biostabilization and Biopreservation. *Annu. Rev. Biomed. Eng.* **2019**, *21*, 1−31.
(51) Cicerone, M. T.; Soles, C. L. Fast Dynamics and Stabilization of Proteins: Binary Glasses of Trehalose and Glycerol. *Biophys. J.* **2004**, *86*, 3836−3845.
(52) Soles, C. L.; Tsai, A. M.; Cicerone, M. T. *Misbehaving Proteins: Protein (Mis)Folding, Aggregation, and Stability*; Springer New York: New York, 2006; pp 193−214, DOI: 10.1007/978-0-387-36063-8_9.
(53) Cornicchi, E.; Onori, G.; Paciaroni, A. Picosecond-Time-Scale Fluctuations of Proteins in Glassy Matrices: The Role of Viscosity. *Phys. Rev. Lett.* **2005**, *95*, 158104.
(54) Wuttke, J.; Budwig, A.; Drochner, M.; Kämmerling, H.; Kayser, F.-J.; Kleines, H.; Ossovyi, V.; Pardo, L. C.; Prager, M.; Richter, D.; Schneider, G. J.; Schneider, H.; Staringer, S. SPHERES, Jülich's high-flux neutron backscattering spectrometer at FRM II. *Rev. Sci. Instrum.* **2012**, *83*, 075109.
(55) Zamponi, M.; Khaneft, M. SPHERES: Backscattering spectrometer. *J. Large-Scale Res. Facil.* **2015**, *1*, A30.
(56) Natali, F.; Peters, J.; Russo, D.; Barbieri, S.; Chiapponi, C.; Cupane, A.; Deriu, A.; Di Bari, M. T.; Farhi, E.; Gerelli, Y.; Mariani, P.; Paciaroni, A.; Rivasseau, C.; Schiro, G.; Sonvico, F. IN13 Backscattering Spectrometer at ILL: Looking for Motions in Biological Macromolecules and Organisms. *Neutron News* **2008**, *19*, 14−18.
(57) Smith, J. C. Protein dynamics: comparison of simulations with inelastic neutron scattering experiments. *Q. Rev. Biophys.* **1991**, *24*, 227−291.
(58) Yi, Z.; Miao, Y.; Baudry, J.; Jain, N.; Smith, J. C. Derivation of Mean-Square Displacements for Protein Dynamics from Elastic Incoherent Neutron Scattering. *J. Phys. Chem. B* **2012**, *116*, 5028−5036.
(59) Parak, F.; Knapp, E. W. A consistent picture of protein dynamics. *Proc. Natl. Acad. Sci. U. S. A.* **1984**, *81*, 7088−7092.
(60) Willis, B.; Pryor, A. *Thermal Vibrations in Crystallography*; Cambridge University Press, 1975.
(61) Zeller, D.; Telling, M. T. F.; Zamponi, M.; García-Sakai, V.; Peters, J. Analysis of elastic incoherent neutron scattering data beyond the Gaussian approximation. *J. Chem. Phys.* **2018**, *149*, 234908.
(62) Frauenfelder, H.; Sligar, S. G.; Wolynes, P. G. The energy landscapes and motions of proteins. *Science* **1991**, *254*, 1598−1603.
(63) Paciaroni, A.; Cinelli, S.; Cornicchi, E.; Francesco, A. D.; Onori, G. Fast fluctuations in protein powders: The role of hydration. *Chem. Phys. Lett.* **2005**, *410*, 400−403.
(64) Schiró, G.; Natali, F.; Cupane, A. Physical Origin of Anharmonic Dynamics in Proteins: New Insights From Resolution-Dependent Neutron Scattering on Homomeric Polypeptides. *Phys. Rev. Lett.* **2012**, *109*, 128102.
(65) Stoeckli, A.; Furrer, A.; Schoenenberger, C.; Meier, B.; Ernst, R.; Anderson, I. Dynamics of hydrogen bonds in carboxylic acids. *Physica B+C* **1986**, *136*, 161−164.
(66) Schiró, G. Anharmonic onsets in polypeptides revealed by neutron scattering: Experimental evidences and quantitative description of energy resolution dependence. *Biophys. Chem.* **2013**, *180*−*181*, 29−36.
(67) Afroze, F.; Nies, E.; Berghmans, H. Phase transitions in the system poly(*N*-isopropylacrylamide)/water and swelling behaviour of the corresponding networks. *J. Mol. Struct.* **2000**, *554*, 55−68.
(68) Van Durme, K.; Van Assche, G.; Van Mele, B. Kinetics of Demixing and Remixing in Poly(N-isopropylacrylamide)/Water Studied by Modulated Temperature DSC. *Macromolecules* **2004**, *37*, 9596−9605.
(69) Buratti, E.; Tavagnacco, L.; Zanatta, M.; Chiessi, E.; Buoso, S.; Franco, S.; Ruzicka, B.; Angelini, R.; Orecchini, A.; Bertoldo, M.; Zaccarelli, E. The role of polymer structure on water confinement in poly(N-isopropylacrylamide) dispersions. *J. Mol. Liq.* **2022**, *355*, 118924.
(70) Ping, Z. H.; Nguyen, Q. T.; Chen, S. M.; Zhou, J. Q.; Ding, Y. D. States of water in different hydrophilic polymers — DSC and FTIR studies. *Polymer* **2001**, *42*, 8461−8467.
(71) Zhang, T.; Li, T.; Nies, E.; Berghmans, H.; Ge, L. Isothermal crystallization study on aqueous solution of poly(vinyl methyl ether) by DSC method. *Polymer* **2009**, *50*, 1206−1213.
(72) Tanaka, M.; Motomura, T.; Ishii, N.; Shimura, K.; Onishi, M.; Mochizuki, A.; Hatakeyama, T. Cold crystallization of water in hydrated poly(2-methoxyethyl acrylate) (PMEA). *Polym. Int.* **2000**, *49*, 1709−1713.
(73) Guan, L.; Xu, H.; Huang, D. The investigation on states of water in different hydrophilic polymers by DSC and FTIR. *Journal of Polymer Research* **2011**, *18*, 681−689.
(74) Guo, Y.; Sun, B.; Wu, P. Phase Separation of Poly(vinyl methyl ether) Aqueous Solution: A Near-Infrared Spectroscopic Study. *Langmuir* **2008**, *24*, 5521−5526.
(75) Nickels, J. D.; O'Neill, H.; Hong, L.; Tyagi, M.; Ehlers, G.; Weiss, K. L.; Zhang, Q.; Yi, Z.; Mamontov, E.; Smith, J. C.; Sokolov, A. P. Dynamics of Protein and its Hydration Water: Neutron Scattering Studies on Fully Deuterated GFP. *Biophys. J.* **2012**, *103*, 1566−1575.
(76) Sebastiani, F.; Longo, M.; Orecchini, A.; Comez, L.; De Francesco, A.; Muthmann, M.; Teixeira, S. C. M.; Petrillo, C.; Sacchetti, F.; Paciaroni, A. Hydration-dependent dynamics of human

telomeric oligonucleotides in the picosecond timescale: A neutron scattering study. *J. Chem. Phys.* **2015**, *143*, 015102.
(77) Russo, D.; Gonzalez, M. A.; Pellegrini, E.; Combet, J.; Ollivier, J.; Teixeira, J. Evidence of Dynamical Constraints Imposed by Water Organization around a Bio−Hydrophobic Interface. *J. Phys. Chem. B* **2013**, *117*, 2829−2836.
(78) Hong, L.; Smolin, N.; Lindner, B.; Sokolov, A. P.; Smith, J. C. Three Classes of Motion in the Dynamic Neutron-Scattering Susceptibility of a Globular Protein. *Phys. Rev. Lett.* **2011**, *107*, 148102.
(79) Schiró, G.; Caronna, C.; Natali, F.; Cupane, A. Direct Evidence of the Amino Acid Side Chain and Backbone Contributions to Protein Anharmonicity. *J. Am. Chem. Soc.* **2010**, *132*, 1371−1376.
(80) Schiró, G.; Caronna, C.; Natali, F.; Cupane, A. Molecular origin and hydration dependence of protein anharmonicity: An elastic neutron scattering study. *Phys. Chem. Chem. Phys.* **2010**, *12*, 10215−10220.
(81) Roh, J. H.; Novikov, V. N.; Gregory, R. B.; Curtis, J. E.; Chowdhuri, Z.; Sokolov, A. P. Onsets of Anharmonicity in Protein Dynamics. *Phys. Rev. Lett.* **2005**, *95*, 038101.
(82) Frick, B.; Fetters, L. J. Methyl Group Dynamics in Glassy Polyisoprene: A Neutron Backscattering Investigation. *Macromolecules* **1994**, *27*, 974−980.
(83) Rasmussen, D. H.; MacKenzie, A. P. Glass transition in amorphous water. Application of the measurements to problems arising in cryobiology. *J. Phys. Chem.* **1971**, *75*, 967−973.
(84) Bohon, R.; Conway, W. DTA studies on the glycerol—water system. *Thermochim. Acta* **1972**, *4*, 321−341.
(85) Hatakeyama, H.; Yoshida, H.; Nakano, J. Studies on the isothermal crystallization of D-glucose and cellulose oligosaccharides by differential scanning calorimetry. *Carbohydr. Res.* **1976**, *47*, 203−211.
(86) Noel, T. R.; Parker, R.; Ring, S. G. A comparative study of the dielectric relaxation behaviour of glucose, maltose, and their mixtures with water in the liquid and glassy states. *Carbohydr. Res.* **1996**, *282*, 193−206.
(87) Shpigelman, A.; Portnaya, I.; Ramon, O.; Livney, Y. D. Saccharide-structure effects on poly N-isopropylacrylamide phase transition in aqueous media; Reflections on protein stability. *J. Polym. Sci., Part B: Polym. Phys.* **2008**, *46*, 2307−2318.
(88) Corezzi, S.; Bracco, B.; Sassi, P.; Paolantoni, M.; Comez, L. Protein Hydration in a Bioprotecting Mixture. *Life* **2021**, *11*, 995.
(89) Shimizu, S.; Smith, D. J. Preferential hydration and the exclusion of cosolvents from protein surfaces. *J. Chem. Phys.* **2004**, *121*, 1148−1154.
(90) Arakawa, T.; Timasheff, S. N. Stabilization of protein structure by sugars. *Biochemistry* **1982**, *21*, 6536−6544.
(91) Zaccai, G. How Soft Is a Protein? A Protein Dynamics Force Constant Measured by Neutron Scattering. *Science* **2000**, *288*, 1604−1607.
(92) Gottfried, D. S.; Peterson, E. S.; Sheikh, A. G.; Wang, J.; Yang, M.; Friedman, J. M. Evidence for Damped Hemoglobin Dynamics in a Room Temperature Trehalose Glass. *J. Phys. Chem.* **1996**, *100*, 12034−12042.
(93) Cicerone, M. T.; Douglas, J. F. $\beta$-Relaxation governs protein stability in sugar-glass matrices. *Soft Matter* **2012**, *8*, 2983−2991.
(94) Lerbret, A.; Affouard, F. Molecular Packing, Hydrogen Bonding, and Fast Dynamics in Lysozyme/Trehalose/Glycerol and Trehalose/Glycerol Glasses at Low Hydration. *J. Phys. Chem. B* **2017**, *121*, 9437−9451.
(95) García-Sakai, V.; Khodadadi, S.; Cicerone, M. T.; Curtis, J. E.; Sokolov, A. P.; Roh, J. H. Solvent effects on protein fast dynamics: implications for biopreservation. *Soft Matter* **2013**, *9*, 5336−5340.




https://doi.org/10.1021/acs.macromol.2c00177
*Macromolecules* 2022, 55, 4752−4765